NIH Public Access
Author Manuscript
Neuroimage. Author manuscript; available in PMC 2016 January 15.

Published in final edited form as:
Neuroimage. 2015 January 15; 105: 462–472. doi:10.1016/j.neuroimage.2014.11.011.

Dynamic Multi-Coil Technique (DYNAMITE) Shimming for Echo-Planar Imaging of the Human Brain at 7 Tesla

Christoph Juchem[*], **S. Umesh Rudrapatna**[*], **Terence W. Nixon**, and **Robin A. de Graaf**
Yale University School of Medicine, Department of Diagnostic Radiology, MR Research Center (MRRC), 300 Cedar Street, New Haven, CT 06520, USA

Abstract

Gradient-echo echo-planar imaging (EPI) is the primary method of choice in functional MRI and other methods relying on fast MRI to image brain activation and connectivity. However, the high susceptibility of EPI towards B_0 magnetic field inhomogeneity poses serious challenges. Conventional magnetic field shimming with low-order spherical harmonic (SH) functions is capable of compensating shallow field distortions, but performs poorly for global brain shimming or on specific areas with strong susceptibility-induced B_0 distortions such as the prefrontal cortex (PFC). Excellent B_0 homogeneity has been demonstrated recently in the human brain at 7 Tesla with the *DYNA*mic *M*ulti-co*I*l *TE*chnique (DYNAMITE) for magnetic field shimming (Juchem et al., J Magn Reson (2011) 212:280-288). Here, we report the benefits of DYNAMITE shimming for multi-slice EPI and T_2* mapping.

A standard deviation of 13 Hz was achieved for the residual B_0 distribution in the human brain at 7 Tesla with DYNAMITE shimming and was 60% lower compared to conventional shimming that employs static zero through third order SH shapes. The residual field inhomogeneity with SH shimming led to an average 8 mm shift at acquisition parameters commonly used for fMRI and was reduced to 1.5-3 mm with DYNAMITE shimming. T_2* values obtained from the prefrontal and temporal cortices with DYNAMITE shimming were 10-50% longer than those measured with SH shimming. The reduction of the confounding macroscopic B_0 field gradients with DYNAMITE shimming thereby promises improved access to the relevant microscopic T_2* effects.

The combination of high spatial resolution and DYNAMITE shimming allows largely artifact-free EPI and T_2* mapping throughout the brain, including prefrontal and temporal lobe areas. DYNAMITE shimming is expected to critically benefit a wide range of MRI applications that rely on excellent B_0 magnetic field conditions including EPI-based fMRI to study various cognitive processes and assessing large-scale brain connectivity *in vivo*. As such, DYNAMITE shimming has the potential to replace conventional SH shim systems in human MR scanners.

© 2014 Elsevier Inc. All rights reserved.

[*]these authors contributed equally

Publisher's Disclaimer: This is a PDF file of an unedited manuscript that has been accepted for publication. As a service to our customers we are providing this early version of the manuscript. The manuscript will undergo copyediting, typesetting, and review of the resulting proof before it is published in its final citable form. Please note that during the production process errors may be discovered which could affect the content, and all legal disclaimers that apply to the journal pertain.

NIH-PA Author Manuscript
NIH-PA Author Manuscript
NIH-PA Author Manuscript

NIH-PA Author Manuscript

NIH-PA Author Manuscript

NIH-PA Author Manuscript

Keywords

shimming; dynamic shimming; echo planar imaging (EPI); multi-coil; spherical harmonics; EPI artifacts

Introduction

MR imaging of neural pathways and functional brain activation is of critical importance to delineate the brain's connectivity *in vivo* and for understanding the manifold computations performed by its neuronal networks during both health and disease.

Functional MRI (fMRI) relies on the repetitive application of fast imaging methods to measure variations in blood oxygen level-dependent (BOLD) contrast (Ogawa et al., 1990) during both external as well as internal stimulation conditions. Echo-planar imaging (EPI) and its many variants are the typical choice at hand, but are highly susceptible to a large collection of potential artifacts including signal dropout and image deformation (Jezzard and Clare, 1999). A prominent weakness of EPI is its vulnerability towards imperfections of the static B_0 magnetic field. Limited field homogeneity remains a long-standing problem for EPI, but also for many other MR methods including steady-state free precession (SSFP) MRI, MR spectroscopic imaging (MRSI) or T_2* mapping. The tissues' intrinsic spin-spin (T_2) relaxation time, for instance, relies on the chemical environment of the tissue water and is further reduced to T_2* by microscopic and macroscopic field alterations. Both the inherent T_2 and the microscopic T_2* contributions carry valuable information with clinical potential (Fernandez-Seara and Wehrli, 2000; Yablonskiy and Haacke, 1994). However, the reduction of the tissues' overall T_2* through large-scale field variations primarily obstructs the view on the relevant, microscopic components.

Diffusion tensor imaging (DTI) employs differences in water diffusivity to derive *in vivo* direct knowledge on tissue microstructure and connectivity (Le Bihan, 2003). DTI typically employs spin-echo EPI as the MRI method of choice, but suffers the same B_0-induced spatial deformations described previously. Moreover, local field imperfections act as additional diffusion gradients in DTI acquisitions and affect the b-matrix in a complex, spatially dependent fashion (Basser and Jones, 2002). Diffusion-based tractography, a primary application of DTI, is based on an mathematically ill-posed problem and faces inherent methodological challenges even for optimal MRI data quality (Jbabdi and Johansen-Berg, 2011; Mangin et al., 2013). Any limitation in image quality or diffusion encoding will inevitably reduce the quality of the attained tractography outcome.

Particularly strong and localized B_0 magnetic field deviations are observed in the prefrontal cortex (PFC) and the temporal lobes (TL). The PFC is involved in many higher order cognitive functions including working memory and cognitive control (Levy and Goldman-Rakic, 2000; Miller et al., 2002). Dysfunction has been linked with many neuropsychiatric illnesses such as bipolar disorder, schizophrenia, or post-traumatic stress disorder (Hains and Arnsten, 2008). Similarly, the TLs are of prime interest due to their role in high-level visual processing (Sigala and Logothetis, 2002) and their relevance for pathologies like temporal lobe epilepsy (Van Paesschen, 2004). The investigation of TL function as well as its

NIH-PA Author Manuscript

NIH-PA Author Manuscript

NIH-PA Author Manuscript

interplay with the rest of the brain is highly desirable, though currently limited by suboptimal TL imaging capabilities in these regions.

Artifacts in EPI and other MR methods susceptible to magnetic field variations can be reduced by the appropriate choice of the MR acquisition parameters (Deichmann et al., 2003; Speck et al., 2008). For instance, improved spatial resolution, i.e. decreased voxel volumes, minimizes intra-voxel magnetic field variations and the resultant signal dephasing. An increased acquisition bandwidth reduces spatial misregistration and image deformation. However, these efforts come at the price of reduced signal-to-noise ratio (SNR), extended acquisition time or increased demands on the scanners' gradient performance. More importantly, any MR investigation relies on optimal parameter choices to derive the most meaningful results for the application at hand. The need to tailor the experimental details to the minimization of artifacts potentially compromises the achievable study outcome.

Post-processing can compensate spatial mis-registration of EPI (Jezzard, 2012) and T_2* mapping (Fernandez-Seara and Wehrli, 2000) to a certain extent. These correction procedures use the residual B_0 field inhomogeneity (Cusack et al., 2003; Jezzard and Balaban, 1995; Weiskopf et al., 2005), the point-spread function (Robson et al., 1997; Zaitsev et al., 2004) or image information acquired with phase-encoding gradients of reversed polarity (Andersson et al., 2003; Morgan et al., 2004) to correct the image distortion at hand. All of these methods, however, require additional reference data or extra scans. More importantly, true signal loss can never be recovered by any post-processing method. Only the experimental minimization of the responsible magnetic field inhomogeneity in a process called magnetic field shimming can provide a true remedy. A complete cancellation of magnetic field variations can be achieved theoretically by superposition of the identical field shape at reversed polarity. In reality, this process is limited by the ability to physically generate the required shim field for the distortion at hand. Deviations between the original field distortion and its best modeling representation inevitably remain as residual field imperfections after the shimming process. Conventional shimming with spherical harmonic (SH) functions is capable of compensating shallow field distortions throughout the brain, but performs poorly in difficult-to-shim areas such as the PFC or for the entire brain (Juchem et al., 2010a; Juchem et al., 2010b; Pan et al., 2012). Dynamic shimming differs from (static) global shimming in that the problem at hand is broken down in subunits. Natural candidates for this approach are the individual slices of multi-slice MRI. The optimization and application of slice-specific field corrections is inherently more powerful than the static use of the identical set of basis shapes irrespective of the method applied. Dynamic SH shimming (DSH) has been used in the human brain to achieve improved magnetic field homogeneity with the application of first (Blamire et al., 1996; Morrell and Spielman, 1997), second (Koch et al., 2006) and third order (Juchem et al., 2010a) SH functions. However, even full third order DSH is not capable to fully mitigate the field imperfections observed in all brain areas and moreover in the PFC.

The ongoing trend towards ultra-high magnetic field imaging is motivated by promises of improved SNR and fMRI contrast behavior. Yet, the expected gains of high field MRI, especially for fMRI and T_2* mapping, have not been fully realized for whole-brain imaging or in difficult-to-shim brain regions at least in part due to the lack of adequate magnetic field

NIH-PA Author Manuscript

NIH-PA Author Manuscript

NIH-PA Author Manuscript

homogenization strategies and technology (Speck et al., 2008). As such, there is a critical need for improved magnetic field homogenization in the human brain.

We have shown recently that excellent magnetic field homogeneity can be achieved in the mouse (Juchem et al., 2011a), the rat (Juchem et al., 2014a) and the human (Juchem et al., 2011b, figure 1) brain with multi-coil (MC) shimming. Basis fields from local, individually driven coils are combined with the MC approach to synthesize the shim field for the problem at hand. The MC shim performance is based on the field modeling capability of the MC approach and further boosted when applied in a dynamic fashion. The aim of this study is to demonstrate the benefits of the *DYNA*mic *M*ulti-co*I*l *TE*chnique (DYNAMITE) for gradient-echo EPI and T_2* mapping of the human brain. Preliminary results of this work have been published in abstract form (Rudrapatna et al., 2014).

Methods

Echo-Planar Imaging and T_2* Mapping

Experiments were performed on a 7 Tesla magnet (Magnex Scientific, Oxford, UK) that was interfaced to a DirectDrive spectrometer and operated with VnmrJ 2.3A software (Agilent Technologies Inc., Santa Clara, CA, USA). The system was equipped with custom-designed, actively-shielded gradients (42 cm ID, 40 mT/m in 512 μs, Magnex Scientific). All experiments used an eight-channel transmit-receive array along with customized B_1-shimming routines. Five healthy volunteers (4 male, 1 female, age 25-45 years) participated in this study in accordance with Institutional Review Board guidelines for the research on human subjects.

EPI was achieved with a customized MR sequence in which sinusoidal k-space trajectories were combined with blipped phase encoding. The reconstruction included 1-dimensional fast Gaussian gridding in the readout direction (Greengard and Lee, 2004), followed by Fourier transformation in the phase encoding direction. The correct reconstruction of non-Cartesian k-space data relies on the exact knowledge of the sampled k-space locations. The theoretical k-space trajectories, however, is typically affected by timing imperfections, eddy-currents and other limitations of the gradient hardware in experimental reality (Mason et al., 1997). The resultant artifacts can be mitigated with the measurement of the applied, physical k-space trajectories and their consideration in the image reconstruction. Here, we tracked the spatio-temporal field behavior with a custom-built 4-channel B_0 field probe array similar to (Barmet et al., 2008) to calibrate and correct the EPI trajectories in this study.

T_2* maps were obtained using a customized multi-gradient-echo MRI sequence. The parameters of both EPI and T_2* maps were chosen to resemble typical fMRI examinations of the human brain at 7 Tesla to illustrate the extent to which image characteristics are affected by B_0 inhomogeneity as a function of image resolution. More specifically, EPI images and T_2* maps were acquired at 3 different isotropic resolutions (3 mm, 2 mm, 1.6 mm) with both SH and DYNAMITE shimming. Gaps were introduced between thinner slices at higher resolution to ensure identical slice positioning and to maintain full brain coverage (field-of-view 20 × 20 cm^2, 13 axial slices, 9 mm slice spacing, radio-frequency bandwidth 1.2 kHz). Note that the decay in transmit efficiency of the RF array for peripheral

NIH-PA Author Manuscript

NIH-PA Author Manuscript

NIH-PA Author Manuscript

(ventral/dorsal) slices was mitigated by slice-specific B_1^+ amplitude scaling with an 8 dB difference between the peripheral and central slices. The EPI images were obtained at TE 30 ms and TR 4.175 s, using sixteen single-shot (readout bandwidth 156 kHz, phase-encode bandwidth 1.42 kHz), eight 2-shot (readout bandwidth 208 kHz, phase-encode bandwidth 2.33 kHz) and four 4-shot (readout bandwidth 227 kHz, phase-encode bandwidth 4.12 kHz) acquisitions for the considered 3 mm, 2 mm and 1.6 mm resolution images, respectively, for matched acquisition durations between conditions. T_2* mapping was based on 6 equidistantly spaced echo times between 4 and 46 ms (readout bandwidth 100 kHz). Identical post-processing was applied for all geometries and both shimming conditions to assure comparability.

Magnetic Field Shimming

Baseline B_0 field distributions were measured with a gradient-echo multi-slice MRI sequence (field-of-view 22 × 22 × 11.7 cm^3, matrix 128 × 64 × 39) at varying echo delays of 0 / 0.33 / 1 / 3 ms. Phase maps were calculated using voxel-by-voxel temporal phase unwrapping, before voxel-specific linear regression of signal phase and echo time was applied to derive 3-dimensional field maps (Juchem et al., 2011a). The decomposition of magnetic fields in the various sets of SH and MC basis fields and the determination of the necessary coil currents for shimming were achieved by constrained least-squares fitting employing the Levenberg-Marquardt algorithm (Juchem et al., 2010c). Magnetic field shimming of any given EPI slice was limited to brain voxels only. A Matlab-based (MathWorks, Natick, MA, USA) software package B0DETOX (‘*beau-detox*’) was established in our laboratory to provide automated image reconstruction, region-of-interest (ROI) selection and magnetic field processing for both SH-based and DYNAMITE shimming (Figure 2). Fully automated brain extraction was achieved with a multi-parametric algorithm that relied on the combination of a series of individual selection criteria with logical AND operations (Juchem et al., 2010b). B0DETOX was operated on the MR scanner console (Linux PC, Intel Core 2, CPU 2.66 GHz, RAM 2 GB) for a streamlined determination of optimal shim settings at minimum user-interaction.

Magnetic field variations within MRI voxels lead to phase cancellation and signal dropout. The consideration of potential (through- or) intra-slice field components is therefore of paramount importance for the successful application of slice shimming. Especially the field artifacts observed in the PFC and the temporal lobes are known to have severe z-components which have motivated the development of z-shimming techniques (Frahm et al., 1988). If shim fields are determined from the 2-dimensional information of a single-slice field map only (Han et al., 2013; Harris et al., 2013), these intra-slice field gradients along the third, through-slice dimension are not considered and inevitably remain in experimental reality. In this study, potential through-slice components were accounted for in the shim optimization by considering narrow 3-dimensional slabs that consisted of the slice-of-interest grouped together with its immediate neighbors similar to previous work (Juchem et al., 2010a; Juchem et al., 2011b).

DYNAMITE basis fields were calibrated individually based on 7 independent 3-dimensional field mapping experiments in a phantom. The experiments covered the dynamic range of the

NIH-PA Author Manuscript

NIH-PA Author Manuscript

NIH-PA Author Manuscript

corresponding current power supply as described previously (Juchem et al., 2011b). DYNAMITE shimming was compared in this study to static, third order SH shimming that was achieved with the scanners' built-in SH coil system with a dynamic range of X 222 Hz/cm, Z 223 Hz/cm, Y 225 Hz/cm, X2-Y2 39.7 Hz/cm^2, ZX 62.0 Hz/cm^2, Z2 52.3 Hz/cm^2, ZY 64.0 Hz/cm^2, XY 40.3 Hz/cm^2, X3 0.27 Hz/cm^3, Z(X2-Y2) 0.74 Hz/cm^3, Z2X 1.14 Hz/cm^3, Z3 3.72 Hz/cm^3, Z2Y 1.18 Hz/cm^3, ZXY 0.75 Hz/cm^3, Y3 0.28 Hz/cm^3 (all linear regression errors <1%).

The effects of SH and DYNAMITE shimming were compared in three different ways: 1) As field homogeneity after theoretical shimming of the B_0 baseline distributions, 2) by analysis of the experimental shim performances within the considered EPI and T_2* slice volumes and 3) via quality outcome measures of the obtained EPI / T_2* results. The magnetic field variations after shimming were characterized with respect to its standard deviation and the frequency spans to cover 80%, 85%, 90% and 95% of the brain voxels (Juchem et al., 2011b). Note that the magnetic field conditions around the EPI / T_2* slice positions were sampled with groups of three 1.6 mm thick slices for the analysis of experimental SH and DYNAMITE shimming. The resultant volumetric field maps allowed the assessment of all remaining intra-slice field dispersion both in-plane and through-plane.

Individual sessions consisted of an initial, unshimmed baseline B_0 map, followed by shimmed B_0 mapping, EPI scans at three resolutions, and T_2* maps at three resolutions. The latter B_0 maps, the EPI and the T_2* mapping experiments were performed twice, once with SH and once with DYNAMITE shimming. The baseline B_0 map was based on single-echo gradient-echo MRI similar to our earlier work (Juchem et al., 2011b) and was used for the calculation of both DYNAMITE and SH shim fields. Magnetic field terms encountered in the human brain are largely shallow with few exceptions in PFC, the temporal lobes and other ventral brain structures. The confined field range with SH / DYNAMITE shimming allowed the application of an accelerated B_0 mapping sequence to measure the shim outcomes. To this end, the regular readout gradient pattern was replaced by a bipolar gradient scheme for multi-echo readout (5 echoes, inter-echo delay 2.64 ms). The duty-cycles for both the read and the slice direction could be balanced more efficiently with this multi-echo approach and shorter acquisition times were achieved with our gradient hardware compared to the single-echo method. Residual phase wrapping was observed in some PFC and TL areas in which the unique frequency range of ±190 Hz was exceeded. They were corrected by a customized spatio-temporal phase unwrapping algorithm. Both the single and the multi-echo B_0 mapping methods provided virtually identical results as confirmed both in phantom experiments and the *in vivo* brain (data not shown). Sessions did not exceed 45 minutes and were tolerated well by all subjects.

Specific DYNAMITE Considerations

DYNAMITE shimming in this study was based on the MC setup described previously (Juchem et al., 2011b). In essence, 48 individual, localized coils (diameter 47 mm, 100 turns) were distributed in 4 rings of 12 coils on the surface of an elliptical former to surround the head of the subjects (Figure 1). The superposition of individual MC fields allowed to resemble the field distortions observed in the human brain and their slice-by-slice

NIH-PA Author Manuscript

NIH-PA Author Manuscript

NIH-PA Author Manuscript

compensation with DYNAMITE shimming. The derived sets of coil currents were uploaded to the MC shim interface via serial RS232 communication and played out during subsequent B_0 field mapping and EPI / T_2* acquisitions based on sequence-initiated TTL triggering signals (Juchem et al., 2011a). In-house developed constant-current amplifier electronics allowed well-defined current alterations over the full dynamic range of ±1 A in less than 200 μs.

DYNAMITE shim fields were updated immediately after the data acquisition from the previous slice. The rapid current alterations with DYNAMITE shimming cause noticeable mechanical vibrations with this prototype implementation. While tolerated well by all subjects (Juchem et al., 2011b), in this study vibrations were further reduced by spreading individual current changes linearly over 5 intermediate steps at 250 μs step-to-step delays. The combined DYNAMITE switching time of approximately 1.5 ms was short compared to the inter-slice (repetition time) delays of approximately 300 ms for the MRI applications in this study. Stable shim field conditions were therefore guaranteed long before the RF excitation of the next slice started and the ramping of coil currents had no effect on the resultant field distributions perceived by the experiment.

Quantification of EPI and T_2* Image Quality

The impact of B_0 shimming on the MRI signal strength was quantitatively assessed in 3 brain areas (PFC, TLs, parietal lobe). EPI image deformations resulting from the residual magnetic field inhomogeneity were then quantified as voxel displacement (Cusack et al., 2003; Jenkinson et al., 2012; Jezzard and Balaban, 1995). Relative changes (DYNAMITE/SH) in T_2* were calculated in a voxel-specific fashion to assess the impact of the two shim conditions on T_2* independent of natural T_2* differences in gray and white matter brain tissue. Voxels representing cerebro-spinal fluid (T_2* > 70 ms) were excluded from this analysis.

Results

Impact of Shimming on the Quality of Echo-Planar Imaging and T_2* Mapping

Global shimming with up to third order SH shapes removed large parts of the shallow field terms encountered in the human brain, but failed to correct the more localized artifacts present in the ventral part of the brain (Fig. 3: ΔB_0, SH). As such, significant field imperfections remained in the PFC and the TLs (slices 3-7). In contrast, DYNAMITE shimming largely improved the magnetic field homogeneity throughout the entire brain (Fig. 3: ΔB_0, DYNAMITE). Moreover, the severe field artifacts in the PFC and the TLs that remained with static SH shimming could be successfully minimized. Overall, the magnetic field variations observed throughout the brain are more closely confined with DYNAMITE compared to SH shimming (Fig. 3: ΔB_0, Histograms).

The quality of EPI and T_2* mapping is significantly reduced with SH shimming in regions of poor B_0 field homogeneity (Fig. 3: EPI SH, T_2* SH). Primarily affected areas include the PFC, the medial TLs, but also the tips of the TLs. While the field distribution is largely homogenous over the bulk of the brain voxels, i.e. inside the brain, a ribbon of gradient

NIH-PA Author Manuscript

NIH-PA Author Manuscript

NIH-PA Author Manuscript

terms at the brain surface cannot be avoided (slices 3-9). The resultant image deformations appear visually pronounced, since the outline of the brain indicated by the red line is altered. Note that this brain outline has been derived from a gradient-echo image with short TE (4 ms) and large acquisition bandwidth (100 kHz) for which spatial deformations are considered small. In contrast, pixels that remain inside the brain when B_0-shifted are more difficult to identify. Such errors are less obvious, but they are by no means less problematic. The residual B_0 distortions after SH shimming in the PFC, however, are so severe that even basic anatomical landmarks such as the anterior horns of the lateral ventricles are rendered unrecognizable (slice 7, arrow). Residual macroscopic B_0 imperfections with SH shimming systematically reduce the apparent T_2* and thereby mask the scientifically and clinically relevant inherent T_2 and microscopic T_2* components (T_2*, SH). Moreover, T_2* alterations are location-specific due to the spatial variations in attainable B_0 homogeneity (ΔB_0, SH).

DYNAMITE shimming successfully mitigated the largest part of the B_0 field inhomogeneity encountered throughout the human brain at 7 Tesla. Large scale field inhomogeneities were eliminated and, more importantly, B_0 imperfections localized in the PFC (slices 6-7) and the TLs (slices 3-5) were strongly reduced. Note that the gradient band surrounding the brain surface after SH shimming (slices 5-9) is avoided with DYNAMITE shimming. As such, the outline of the brain imaged with single-shot EPI is largely preserved as signal bleeding from brain to non-brain areas (and vice versa) is avoided. Similarly, the tissue topology inside the brain remains intact and anatomical features such as the frontal horns of the lateral ventricles can be clearly identified (slice 7, arrow). In the same vein, T_2* mapping benefits from both spatial accuracy and reduced macroscopic relaxivity (T_2*, DYNAMITE). The most severe and localized field terms cannot be completely eliminated with the current DYNAMITE installation (slice 6) and lead to some T_2* reduction and signal pile-up with EPI.

Similar B_0 homogeneity, EPI quality and T_2* results were obtained in all 5 subjects (Fig. 4). More specifically, significant B_0 imperfections remained after SH shimming throughout the brain and especially in the PFC (ΔB_0, SH). Consequently, both EPI fidelity (EPI, SH) and T_2* mapping (T_2*, SH) suffered from the residual B_0 inhomogeneity. In contrast, DYNAMITE shimming largely eliminated B_0 field inhomogeneity throughout the brain (ΔB_0, DYNAMITE), spatial misregistration was minimized and the brains' outline was preserved (EPI, DYNAMITE). In the same vein, prolonged T_2* values were obtained with DYNAMITE shimming in brain regions that suffered from poor B_0 homogeneity with SH shimming (T_2*, DYNAMITE). This minimization of the macroscopic T_2* contributions clears the view on microscopic, i.e. tissue-specific, contributions at hand even in the PFC and TLs.

As expected, increased image resolution and the concomitant reduction of voxel volumes potentially suffering from phase cancellation was found to reduce image deformation and signal dropout. However, spatial misregistration and alterations of the brain outline were observed even at the highest spatial resolution applied in this study (4-shot: EPI). Similarly, high resolution did not fully mitigate T_2* reductions due to macroscopic B_0 imperfections (4-shot: T_2*). DYNAMITE shimming was able to provide an additional benefit in both EPI fidelity and T_2* mapping irrespective of the applied image resolution. Only the combination

NIH-PA Author Manuscript

NIH-PA Author Manuscript

NIH-PA Author Manuscript

of high resolution and DYNAMITE shimming was found to completely mitigate B_0-induced EPI and T_2* mapping artifacts (4-shot: EPI/T_2*, DYNAMITE).

Brain areas such as the parietal lobe in which homogeneous B_0 field conditions could be achieved with both shimming methods revealed similar T_2* values corresponding to a T_2* ratio DYNAMITE/SH close to 1 (Fig. 6, Parietal). Note that the average value and the standard deviations of a T_2* distribution are susceptible to outliers. Therefore, the median and the median absolute deviation of the ratio of T_2* values are considered here as measures of regional T_2* variations. The improved B_0 field homogeneity in difficult-to-shim areas such as the PFC and the TLs with DYNAMITE resulted in prolonged T_2* values and increased T_2* ratios (Fig. 6, Prefrontal/Temporal). As expected, the largest improvements were found at the coarsest resolution. More specifically, the T_2* ratio increased by approximately 40% in the TLs and 20% in the PFC at an isotropic 3-mm resolution. Although the effect becomes less pronounced at finer spatial resolution, even at the highest 1.6 mm isotropic resolution DYNAMITE-shimmed T_2* times were approximately 20% longer in the TLs and 10% longer in the PFC compared to SH shimming.

Similarly, the regional analysis of the EPI image fidelity revealed negligible median pixel shifts along the phase-encode direction in the parietal lobe irrespective of the spatial resolution as adequate B_0 homogeneity was achieved in this brain region with both shimming methods (Fig. 7, Parietal, median value ± median absolute deviation). In the PFC and the TLs, EPI images acquired at 3 mm resolution exhibited a typical shift of approximately 8 mm with SH shimming which was further reduced to 3 mm with DYNAMITE shimming. Moreover, pixel-to-pixel variations, i.e. the spread of pixel shifts within the region at hand, could be largely reduced with DYNAMITE shimming and confined to a narrower range (Fig. 7, Prefrontal/Temporal, error bars). Improved image resolution resulted in similar reductions of the overall pixel shift and the range of pixel shifts encountered regionally (Fig. 7, 3 mm/2 mm/1.6 mm). However, only the combination of DYNAMITE shimming and high 1.6 mm spatial resolution allowed negligible pixels shifts in the PFC and the TLs.

Magnetic Field Shimming of the Human Brain at 7 Tesla

Similar improvements in whole brain B_0 homogeneity were achieved for all 5 subjects and reflected in 62% and 67% average reductions in the standard deviation of field values after shimming and all frequency width measures, respectively (Table 1).

All SH and DYNAMITE shim fields were calculated and applied in a single-step process, i.e. multiple iterations were not necessary. The theoretical DYNAMITE and SH shimming results were confirmed in its experimental realization (Table 2) and are in agreement with previous work (Juchem et al., 2011b).

Discussion

The impact of magnetic field homogeneity provided by SH and DYNAMITE shimming on the image fidelity of EPI and T_2* maps was analyzed in this study. SNR and image quality of both EPI and T_2* mapping benefited from DYNAMITE shimming. DYNAMITE

NIH-PA Author Manuscript

NIH-PA Author Manuscript

NIH-PA Author Manuscript

shimming reduced the overall image distortions typically observed with conventional SH shimming and enabled reasonable SNR even in areas of complex field disturbance. The residual field deviations after DYNAMITE shimming are predictable and, therefore, further improvements in image quality are expected with their consideration in the spatial reconstruction (Cusack et al., 2003; Jezzard and Balaban, 1995; Zeng and Constable, 2002). Notably, spatial misregistration tends to be visually most noticeable if the brain's outline is affected. While voxels from the brain center might be equally affected, their continuance within the brain might be misinterpreted as improved registration accuracy. In the human brain, the most severe field inhomogeneities are found well within the brain and spatial misregistration within the brain is the rule rather than the exception.

Due to the numerous geometric conditions applied in this research and the limited experiment time per study, the decision was made to experimentally compare DYNAMITE shimming to static third order SH shimming as a compromise between basic shimming capabilities and state-of-the-art third order DSH that is currently available in only a very limited number of laboratories world-wide. The entire brain was considered in the theoretical comparison of shim methods (Table 1), whereas Table 2 is based on groups of 3 slices to resemble the geometry used for EPI and T_2* mapping. While both data sets refer to the same subjects and experiment sessions, the details of the field analysis somewhat depend on the ROI selection. The latter included the computational brain extraction along with a selection of basic quality measures to ensure the consideration of meaningful field values only (Juchem et al., 2010b). However, identical ROIs were applied for the comparison of DYNAMITE and SH shimming in both the theoretical and the experimental analysis and, therefore, all reported results are inherently consistent.

The theoretical comparison of DYNAMITE shimming with static and dynamic SH shimming up to the fifth and fourth order, respectively, demonstrates its superiority in line with previous work (Juchem et al., 2011b). In this analysis, theoretical DYNAMITE shimming was based on the set of MC basis fields that were obtained experimentally and these MC shapes resembled their theoretical predictions with a high degree of similarity (data not shown, Juchem et al., 2011b). More importantly, this approach ensured that the employed MC field shapes are experimentally available and that all further conditions, such as the apparent current limitation of the applied amplifier hardware, are considered correctly. In contrast, theoretical SH field modeling and shimming was based on the theoretical SH field shapes and an infinite dynamic range was assumed for all terms. While the premise of sufficient amplitude range might not hold for every implementation, it ensured the generality of the obtained results. Moreover, the residual field inhomogeneity is independent of the available SH amplitude range and therefore a sole consequence of the underlying magnetic field shaping. The reduction in field inhomogeneity with the current implementation of DYNAMITE shimming is expected to be double of that achievable with fifth order static SH shimming and is predicted to outperform even fourth order dynamic SH shimming (Table 1). In other words, DYNAMITE shimming provides significant overall improved magnetic field homogeneity and is particularly versatile for the limitation of localized, non-trivial terms as observed in the PFC (Figs. 3/4). Current DSH implementations are based on bore-sized SH coils. They face technical challenges, e.g. the generation of eddy currents, which are negligible for the presented DYNAMITE approach.

NIH-PA Author Manuscript

NIH-PA Author Manuscript

NIH-PA Author Manuscript

The extension of DSH to the fourth order is therefore a non-trivial task. In addition, the net gain per inclusion of additional SH orders has been shown to become progressively smaller for higher SH orders (Juchem et al., 2010a) which might be another reason why fourth order DSH has not been presented yet. Low order SH shapes are a subsection of the repertoire of field shapes that can be generated with current MC technology (e.g. Juchem et al., 2013). As such, there is no incentive for the combination of (D)SH and DYNAMITE shimming as no significant net benefit is achieved compared to DYNAMITE shimming alone.

The implementation of DYNAMITE for B_0 shimming of the human brain requires three major components: 1) The MC setup capable of providing shim fields that resemble B_0 distortions encountered in the human brain, 2) software and algorithms for MC magnetic field modeling and the calculation of DYNAMITE shim fields and 3) multi-amplifier electronics to drive and update individual MC channels for the generation of slice-specific shim fields in a dynamic fashion. All software and hardware applied in this study has been custom-designed and – built. The rapidly increasing interest in MC technology for both B_0 shimming and imaging (Juchem et al., 2014b; Juchem et al., 2012), however, is expected to promote access and distribution of methods, and the potential development of commercially available solutions.

The calculation of DYNAMITE shim fields is conceptually similar to dynamic B_0 shimming with SH shapes, i.e. DSH. The brain ROI at hand is broken down into a series of narrow 3-dimensional slabs which are analyzed individually. The computational burden for DYNAMITE shimming is somewhat higher as more and non-orthogonal basis shapes are used. While one shim analysis for every slice is needed with dynamic shimming, the time requirement per fit is smaller due to the largely reduced ROI volume and the dimensionality of the numerical optimization problem. In this study, the overall time penalty for DYNAMITE processing of 13 slices compared to the calculation of global third order SH shim fields was 2-2.5 minutes (figure 2) on a low performance linux PC with methods that have not been optimized for speed. Improved computational resources and the translation of the Matlab routines to a more efficient software environment, such as C++, are expected to largely reduce the processing times. In addition, the numerical optimization problem is linear in nature and parallel processing strategies promise further multifold gains in processing speed.

While DYNAMITE shimming mitigated the largest part of the B_0 imperfections encountered in the human brain at 7 Tesla, some extreme disturbances were beyond the modeling capability of the applied DYNAMITE implementation and could not be fully compensated. For instance, the ventral end of the field focus in the PFC directly above the sinus cavities was found to be extremely localized and steep (Fig. 3, ΔB_0, slice 6). In combination with its position inside the brain, a complete homogenization along with the rest of the axial slice was not achieved with the current DYNAMITE implementation. Potential remedies include improvements of the MC modeling capacity by increasing the available amplitude range per MC channel (Juchem et al., 2013) and a further extension/ optimization of the MC assembly in future designs.

NIH-PA Author Manuscript

NIH-PA Author Manuscript

NIH-PA Author Manuscript

Subject motion and head displacements are a problem for every shimming method and almost every MR method. The spatial complexity of the apparent field distortions in the human brain, e.g. in the PFC, requires shim fields of equal complexity and spatial specificity for their compensation. Therefore, any shim method, DYNAMITE or SH, that achieves good compensation has equal sensitivity to motion. The correction of motion-induced B_0 alterations has not been investigated here, but the short switching times of the current implementation (200 μs, full range) are expected to support the real-time compensation of motion-induced (Hess et al., 2011; Ward et al., 2002) or respiration-induced (van Gelderen et al., 2007) B_0 alterations. However, the feasibility of real-time DYNAMITE shimming is yet to be demonstrated.

DYNAMITE shimming, like any other active shimming method, relies on driving conducting wire patterns with electrical current. The resultant energy deposition and concomitant heat generation have not been problematic in previous DYNAMITE applications even though no active cooling was applied (Juchem et al., 2011b). Here, the average current over all 48 coils and the 13 slices of the EPI acquisitions across subjects was (0.38 ± 0.03) A. In other words, similar duty cycles were observed in all subjects. The spread of coil currents per subject, i.e. its SD, was also similar across subjects with an average of (0.35 ± 0.01) A. Notably, the coils' current load showed a strong bias towards the ventral slices for which complex and high amplitude shim shapes needed to be generated. The channel with the highest duty cycle, i.e. the worst case, was different for every subject, however, at similar current load of (0.72 ± 0.03) A. Temperature rises due to coil heating remained below 15 degrees Celsius at all times and absolute coil temperatures stayed well below 37 degrees Celsius, i.e. body temperature, at all times (data not shown).

In its current implementation, the DYNAMITE shim field for the next EPI slice to be imaged is applied immediately after the sampling of the earlier slice has been completed. In other words, one of the 13 shim fields is applied at all times and the series of slice-specific shim fields is cycled with an effective on-time of 100%. If necessary, the effective on-time and the concomitant temperature rise can be reduced by inclusion of intermediate time windows during which no fields are applied. Neither the MRI sequence timing nor the experimental results are compromised with this approach, but multifold reductions of the resultant duty cycles, e.g. approximately 10-fold for the EPI sequence parameters applied in this study, are expected.

MC basis fields were characterized in a single calibration session and used for all subjects. The accuracy of the MC field generation critically relies on the exact knowledge of the position of the MC setup within the magnet and was therefore measured relative to the calibration study for every subject and session. The knowledge derived by this 1-minute experiment was used in the proof-of-principle study (Juchem et al., 2011b) to physically reposition the MC setup by means of moving the patient bed it was mounted on. In this study, the position of neither the bed nor the MC setup were altered after they had been brought into the magnet. Instead, positioning discrepancies between the study and the MC calibration experiment were considered by coordinate transformation of the original calibration MC basis set at an accuracy of approximately 1 mm. Notably, this procedure also included a potential re-gridding to arbitrary MRI geometries and thereby provided full

NIH-PA Author Manuscript

NIH-PA Author Manuscript

NIH-PA Author Manuscript

flexibility for both the calibration experiment and the application of DYNAMITE shimming for EPI and T_2* mapping.

The integration of DYNAMITE B_0 shimming with the available transmit-receive RF array allows EPI-based fMRI of the default network and certain stimulation paradigms (e.g. motor tasks, data not shown). Room around the head is particularly precious in fMRI studies with visual stimulation paradigms due to the conflicting space requirements of multi-channel RF arrays, stimulation devices such as mirrors or prism optics and potential further hardware to track head and/or eye movements. While the MC setup represents yet another piece of hardware, the benefits of DYNAMITE shimming for EPI and T_2* mapping – especially in the PFC and the TLs – warrant its integration through a net gain in MRI quality and derivable information content. The MC approach does not critically rely on the details of individual basis fields and the underlying coil geometries, and allowed the integration of the RF and MC technology in the presented work. More importantly, a centered 10-cm band around the subjects' eyes remained free of shim coils (compare figure 1) and could be used for visual stimulation and/or eye tracking. While an engineering challenge, we do not foresee any fundamental obstacles for the dedicated integration of MC, RF, stimulation and tracking hardware that will allow fMRI investigations with visual stimulation paradigms to benefit from DYNAMITE shimming. Notably, the front part of the MC setup applied in this study is removable for easier subject access and placement. This functionality could not be used, however, since the surrounding RF coil could not be opened in a similar fashion. The need for study subjects to slide into the prototype MC/RF setup limits subject comfort and restricts its suitability for studying elderly and patients. The use of modular RF coils (Avdievich, 2011) in future MC/RF designs is expected to render this limitation obsolete.

DYNAMITE shimming enables excellent B_0 magnetic field conditions throughout the brain. The MC setup was designed to benefit MR investigations targeting the *in vivo* human brain at 7 Tesla and improved quality of EPI and T_2* mapping has been demonstrated. This is the first application-driven study employing DYNAMITE shimming in the *in vivo* human brain. The developed technology and methods promise to prove equally beneficial for other multi-slice MR applications that require a high degree of magnetic field homogeneity, such as steady-state free precession MRI, diffusion tensor imaging or multi-slice MR spectroscopic imaging. DYNAMITE shimming is expected to benefit MR investigations that aim at full brain coverage for activation and functional connectivity assessment including studies on multi-sensory and motor interactions, higher-order cognitive processing or the default network. Along with the efficiency gains of MC-based shimming compared to SH approaches shown recently (Juchem et al., 2013), the MC technology has the potential to replace conventional SH shim systems for magnetic field shimming in the human brain.

Acknowledgments

The authors thank Dr. John Onophrey for helpful discussions on brain segmentation and for sharing the BioimageSuite (www.bioimagesuite.org) implementation of the Brain Extraction Tool (BET, (Smith, 2002)). This research was supported by NIH grants P30-NS052519, R01-EB000473 and R01-EB014861.

NIH-PA Author Manuscript

NIH-PA Author Manuscript

NIH-PA Author Manuscript

References

Andersson JL, Skare S, Ashburner J. How to correct susceptibility distortions in spin-echo echo-planar images: application to diffusion tensor imaging. Neuroimage. 2003; 20:870–888. [PubMed: 14568458]

Avdievich NI. Transceiver-Phased Arrays for Human Brain Studies at 7 T. Appl Magn Reson. 2011; 41:483–506. [PubMed: 23516332]

Barmet C, De Zanche N, Pruessmann KP. Spatiotemporal magnetic field monitoring for MR. Magn Reson Med. 2008; 60:187–197. [PubMed: 18581361]

Basser PJ, Jones DK. Diffusion-tensor MRI: theory, experimental design and data analysis - a technical review. NMR Biomed. 2002; 15:456–467. [PubMed: 12489095]

Blamire AM, Rothman DL, Nixon T. Dynamic shim updating: a new approach towards optimized whole brain shimming. Magn Reson Med. 1996; 36:159–165. [PubMed: 8795035]

Cusack R, Brett M, Osswald K. An evaluation of the use of magnetic field maps to undistort echo-planar images. Neuroimage. 2003; 18:127–142. [PubMed: 12507450]

Deichmann R, Gottfried JA, Hutton C, Turner R. Optimized EPI for fMRI studies of the orbitofrontal cortex. Neuroimage. 2003; 19:430–441. [PubMed: 12814592]

Fernandez-Seara MA, Wehrli FW. Postprocessing technique to correct for background gradients in image-based R*(2) measurements. Magn Reson Med. 2000; 44:358–366. [PubMed: 10975885]

Frahm J, Merboldt KD, Hanicke W. Direct FLASH MR imaging of magnetic field inhomogeneities by gradient compensation. Magn Reson Med. 1988; 6:474–480. [PubMed: 3380007]

Greengard L, Lee JY. Accelerating the Nonuniform Fast Fourier Transform. SIAM J Appl Math. 2004; 46:443–454.

Hains AB, Arnsten AF. Molecular mechanisms of stress-induced prefrontal cortical impairment: implications for mental illness. Learn Mem. 2008; 15:551–564. [PubMed: 18685145]

Han H, Song AW, Truong TK. Integrated parallel reception, excitation, and shimming (iPRES). Magn Reson Med. 2013; 70:241–247. [PubMed: 23629974]

Harris CT, Handler WB, Chronik BA. A new approach to shimming: The dynamically controlled adaptive current network. Magn Reson Med. 2013

Hess AT, Dylan Tisdall M, Andronesi OC, Meintjes EM, van der Kouwe AJ. Real-time motion and B(0) corrected single voxel spectroscopy using volumetric navigators. Magn Reson Med. 2011

Jbabdi S, Johansen-Berg H. Tractography: where do we go from here? Brain Connect. 2011; 1:169–183. [PubMed: 22433046]

Jenkinson M, Beckmann CF, Behrens TE, Woolrich MW, Smith SM. FSL. Neuroimage. 2012; 62:782–790. [PubMed: 21979382]

Jezzard P. Correction of geometric distortion in fMRI data. Neuroimage. 2012; 62:648–651. [PubMed: 21945795]

Jezzard P, Balaban RS. Correction for geometric distortion in echo planar images from B0 field variations. Magn Reson Med. 1995; 34:65–73. [PubMed: 7674900]

Jezzard P, Clare S. Sources of distortion in functional MRI data. Hum Brain Mapp. 1999; 8:80–85. [PubMed: 10524596]

Juchem C, Brown PB, Nixon TW, McIntyre S, Rothman DL, de Graaf RA. Multi-coil shimming of the mouse brain. Magn Reson Med. 2011a; 66:893–900. [PubMed: 21442653]

Juchem C, Green D, de Graaf RA. Multi-coil magnetic field modeling. J Magn Reson. 2013; 236:95–104. [PubMed: 24095841]

Juchem C, Herman P, Sanganahalli BG, Nixon TW, Brown PB, McIntyre S, Hyder F, de Graaf RA. Dynamic Multi-Coil Technique (DYNAMITE) Shimmed EPI of the Rat Brain at 11.7 Tesla. NMR Biomed. 2014a; 27:897–906. [PubMed: 24839167]

Juchem, C.; Nahhass, OM.; Nixon, TW.; de Graaf, RA. Proc ISMRM. Milan, Italy: 2014b. 3D MR Imaging with the Dynamic Multi-Coil Technique: DYNAMITE MRI; p. 0930

Juchem, C.; Nixon, TW.; de Graaf, RA. Proc ISMRM. Melbourne, Australia: 2012. Multi-Coil Imaging with Algebraic Reconstruction; p. 2545

NIH-PA Author Manuscript NIH-PA Author Manuscript NIH-PA Author Manuscript

Juchem C, Nixon TW, Diduch P, Rothman DL, Starewicz P, de Graaf RA. Dynamic shimming of the human brain at 7 Tesla. Concepts Magn Reson. 2010a; 37B:116–128.

Juchem C, Nixon TW, McIntyre S, Boer VO, Rothman DL, de Graaf RA. Dynamic multi-coil shimming of the human brain at 7 Tesla. J Magn Reson. 2011b; 212:280–288. [PubMed: 21824794]

Juchem C, Nixon TW, McIntyre S, Rothman DL, de Graaf RA. Magnetic field homogenization of the human prefrontal cortex with a set of localized electrical coils. Magn Reson Med. 2010b; 63:171–180. [PubMed: 19918909]

Juchem C, Nixon TW, McIntyre S, Rothman DL, de Graaf RA. Magnetic field modeling with a set of individual localized coils. J Magn Reson. 2010c; 204:281–289. [PubMed: 20347360]

Koch KM, McIntyre S, Nixon TW, Rothman DL, de Graaf RA. Dynamic shim updating on the human brain. J Magn Reson. 2006; 180:286–296. [PubMed: 16574443]

Le Bihan D. Looking into the functional architecture of the brain with diffusion MRI. Nat Rev Neurosci. 2003; 4:469–480. [PubMed: 12778119]

Levy R, Goldman-Rakic PS. Segregation of working memory functions within the dorsolateral prefrontal cortex. Exp Brain Res. 2000; 133:23–32. [PubMed: 10933207]

Mangin JF, Fillard P, Cointepas Y, Le Bihan D, Frouin V, Poupon C. Toward global tractography. Neuroimage. 2013; 80:290–296. [PubMed: 23587688]

Mason GF, Harshbarger T, Hetherington HP, Zhang Y, Pohost GM, Twieg DB. A method to measure arbitrary k-space trajectories for rapid MR imaging. Magn Reson Med. 1997; 38:492–496. [PubMed: 9339451]

Miller EK, Freedman DJ, Wallis JD. The prefrontal cortex: categories, concepts and cognition. Philos Trans R Soc Lond B Biol Sci. 2002; 357:1123–1136. [PubMed: 12217179]

Morgan PS, Bowtell RW, McIntyre DJ, Worthington BS. Correction of spatial distortion in EPI due to inhomogeneous static magnetic fields using the reversed gradient method. J Magn Reson Imaging. 2004; 19:499–507. [PubMed: 15065175]

Morrell G, Spielman D. Dynamic shimming for multi-slice magnetic resonance imaging. Magn Reson Med. 1997; 38:477–483. [PubMed: 9339449]

Ogawa S, Lee TM, Kay AR, Tank DW. Brain magnetic resonance imaging with contrast dependent on blood oxygenation. Proc Natl Acad Sci U S A. 1990; 87:9868–9872. [PubMed: 2124706]

Pan JW, Lo KM, Hetherington HP. Role of high order and degree B(0) shimming for spectroscopic imaging of the human brain at 7 tesla. Magn Reson Med. 2012; 68:1007–1017. [PubMed: 22213108]

Robson MD, Gore JC, Constable RT. Measurement of the point spread function in MRI using constant time imaging. Magn Reson Med. 1997; 38:733–740. [PubMed: 9358447]

Rudrapatna, SU.; Nixon, WT.; McIntyre, S.; de Graaf, RA.; Juchem, C. Proc ISMRM. Melbourne, Australia: 2014. Improved EPI at 7T with Dynamic Multi-Coil Technique (DYNAMITE) Shimming; p. 0931

Sigala N, Logothetis NK. Visual categorization shapes feature selectivity in the primate temporal cortex. Nature. 2002; 415:318–320. [PubMed: 11797008]

Smith SM. Fast robust automated brain extraction. Hum Brain Mapp. 2002; 17:143–155. [PubMed: 12391568]

Speck O, Stadler J, Zaitsev M. High resolution single-shot EPI at 7T. MAGMA. 2008; 21:73–86. [PubMed: 17973132]

van Gelderen P, de Zwart JA, Starewicz P, Hinks RS, Duyn JH. Real-time shimming to compensate for respiration-induced B0 fluctuations. Magn Reson Med. 2007; 57:362–368. [PubMed: 17260378]

Van Paesschen W. Qualitative and quantitative imaging of the hippocampus in mesial temporal lobe epilepsy with hippocampal sclerosis. Neuroimaging Clin N Am. 2004; 14:373–400. vii. [PubMed: 15324854]

Ward HA, Riederer SJ, Jack CR Jr. Real-time autoshimming for echo planar timecourse imaging. Magn Reson Med. 2002; 48:771–780. [PubMed: 12417991]

NIH-PA Author Manuscript

NIH-PA Author Manuscript

NIH-PA Author Manuscript

Weiskopf N, Klose U, Birbaumer N, Mathiak K. Single-shot compensation of image distortions and BOLD contrast optimization using multi-echo EPI for real-time fMRI. Neuroimage. 2005; 24:1068–1079. [PubMed: 15670684]

Yablonskiy DA, Haacke EM. Theory of NMR signal behavior in magnetically inhomogeneous tissues: the static dephasing regime. Magn Reson Med. 1994; 32:749–763. [PubMed: 7869897]

Zaitsev M, Hennig J, Speck O. Point spread function mapping with parallel imaging techniques and high acceleration factors: fast, robust, and flexible method for echo-planar imaging distortion correction. Magn Reson Med. 2004; 52:1156–1166. [PubMed: 15508146]

Zeng H, Constable RT. Image distortion correction in EPI: comparison of field mapping with point spread function mapping. Magn Reson Med. 2002; 48:137–146. [PubMed: 12111941]

NIH-PA Author Manuscript

NIH-PA Author Manuscript

NIH-PA Author Manuscript

Highlights

- DYNAMITE shimming provides high level B_0 homogeneity throughout the human brain
- DYNAMITE shimming outperforms conventional spherical harmonics shimming
- Signal dropout and pixel misregistration of echo-planar imaging (EPI) are minimized
- Removal of macroscopic field gradients improves mapping of microscopic T2* effects
- DYNAMITE shimming is expected to benefit a wide range of brain MR I applications

NIH-PA Author Manuscript

NIH-PA Author Manuscript

NIH-PA Author Manuscript

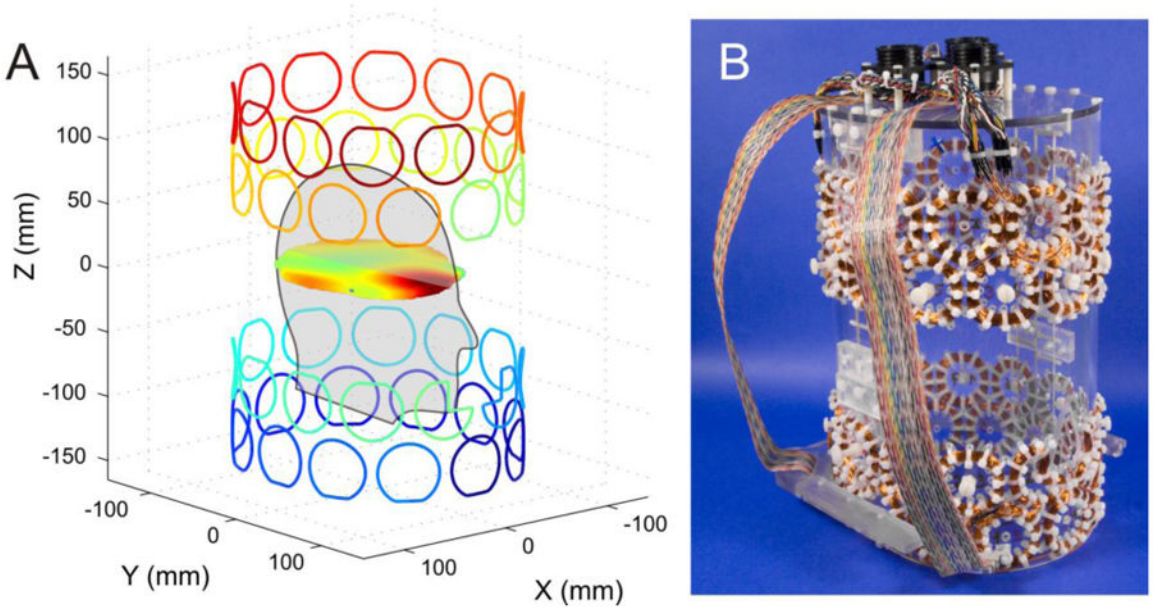

Fig. 1.

Theoretical design (A) and experiment realization (B) of the 48-channel multi-coil setup for magnetic field homogenization of the human brain at 7 Tesla. DYNAMITE shimming in axial slices was achieved through superposition of the 48 basis field shapes that were generated by this matrix of independently driven, localized coils (adopted from Juchem C et al., JMR 212:280-288 (2011)).

NIH-PA Author Manuscript
NIH-PA Author Manuscript
NIH-PA Author Manuscript

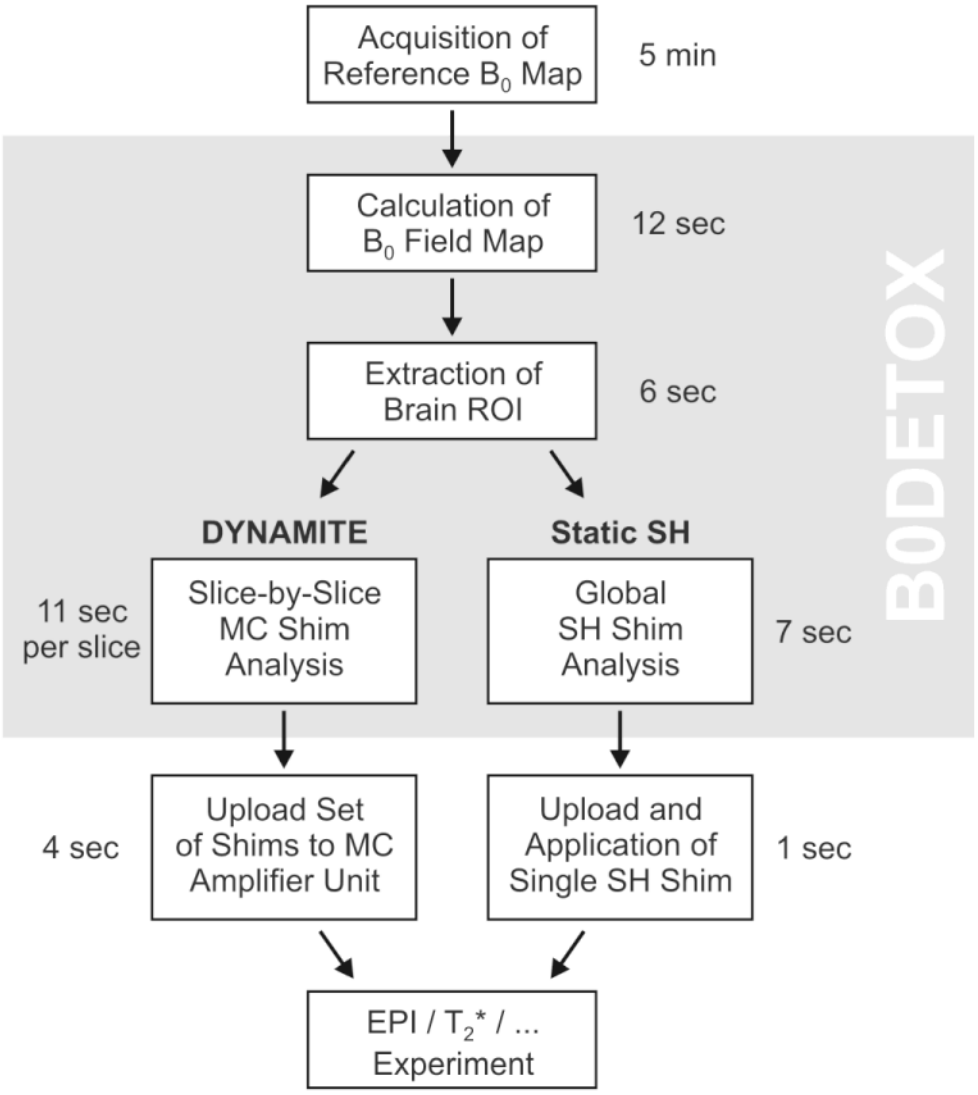

Fig. 2.
Time requirements of DYNAMITE and static SH shimming for EPI/T2* investigations.

NIH-PA Author Manuscript
NIH-PA Author Manuscript
NIH-PA Author Manuscript

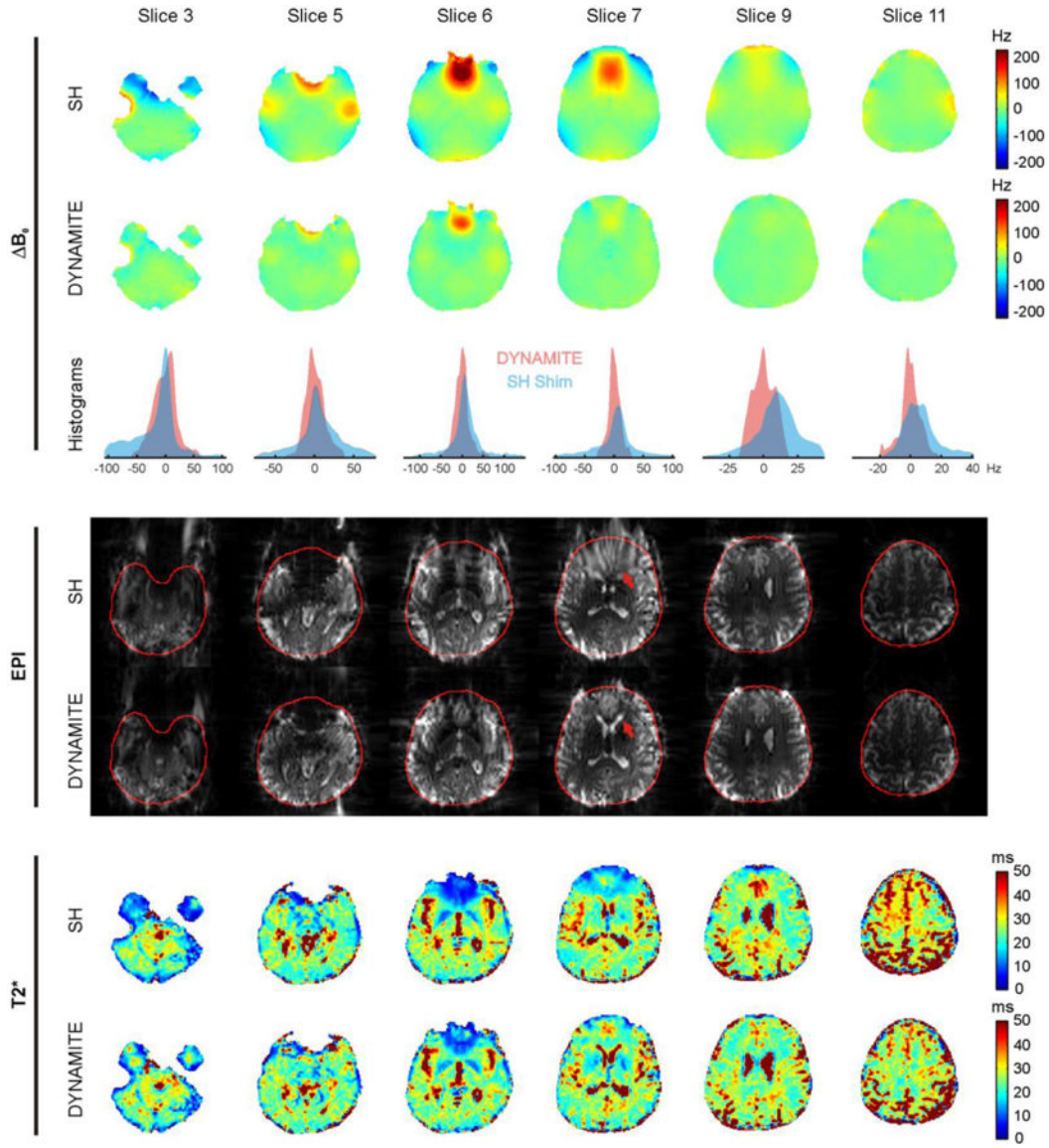

Fig. 3.

Impact of DYNAMITE/SH shimming on the quality of EPI and T_2* mapping of the human brain at 7 Tesla. SH shimming is capable of removing the shallow terms, but fails to compensate localized field terms in the prefrontal cortex, the temporal lobes and at the brain surface (ΔB_0, SH). DYNAMITE shimming further mitigates shallow and, moreover, localized field components in axial slices throughout the brain (ΔB_0, DYNAMITE). The improved field compensation with DYNAMITE shimming is reflected in more narrow frequency distributions compared to SH shimming (B0 Histogram). Improved B0 field homogeneity with DYNAMITE shimming results in improved EPI quality (EPI, DYNAMITE) compared to conventional shimming (EPI, SH). More specifically, signal dropouts are reduced and pixel misregistration both inside the brain and at the brain surface are minimized. While reduced T_2* values are observed in areas of significant B_0

inhomogeneity with SH shimming (T_2*, SH), these effects are minimized with DYNAMITE shimming (T_2*, DYNAMITE).

NIH-PA Author Manuscript
NIH-PA Author Manuscript
NIH-PA Author Manuscript

NIH-PA Author Manuscript

NIH-PA Author Manuscript

NIH-PA Author Manuscript

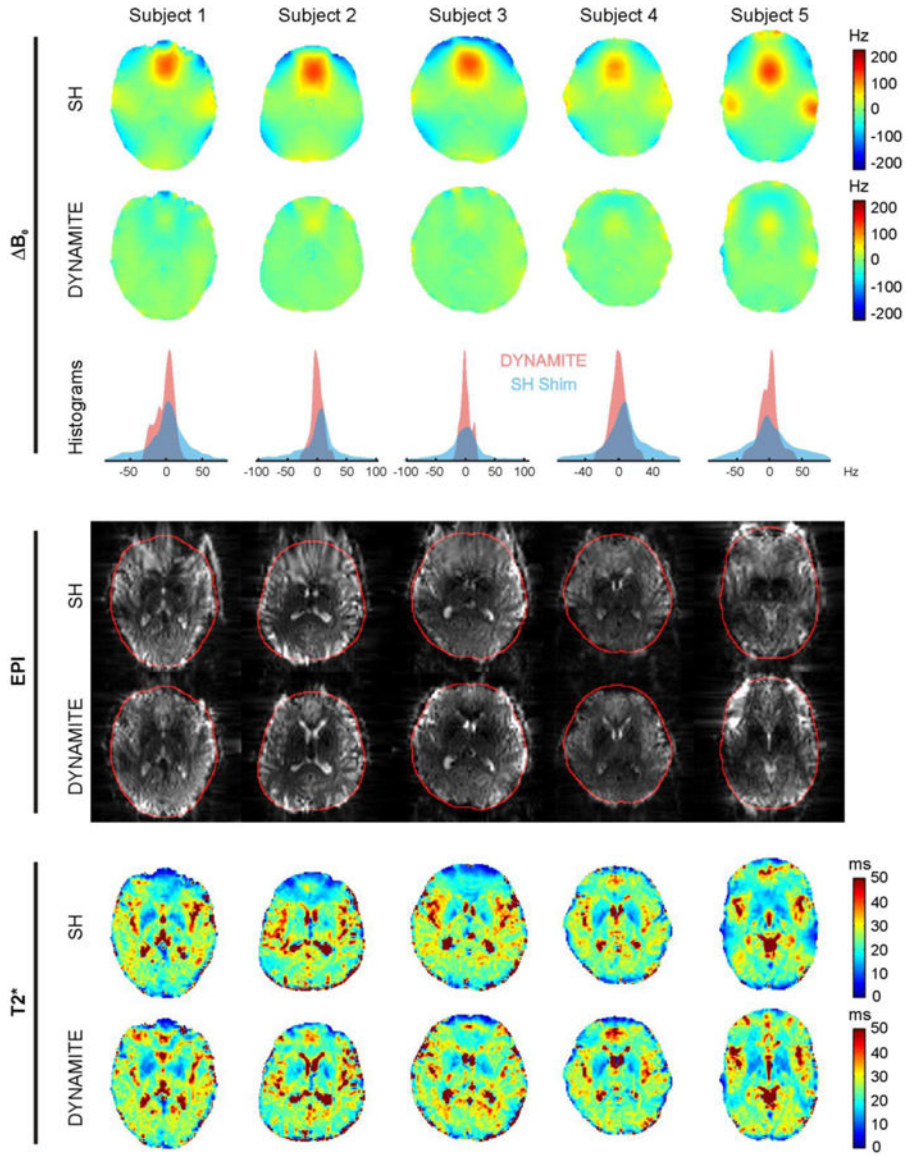

Fig. 4.

EPI and T_2* mapping quality with DYNAMITE and SH shimming across all 5 subjects of the study. Severe field imperfections remain in the PFC with third order SH shimming (ΔB_0, SH), but are largely erased with DYNAMITE shimming (ΔB_0, DYNAMITE). Improved B_0 conditions with DYNAMITE shimming minimized spatial misregistration of EPI (EPI, DYNAMITE), preserved the outline of the brain (red line) and maintained the structural topology of anatomical features inside the brain. DYNAMITE-shimmed T_2* maps showed reduced T_2* shortening from macroscopic field gradients in areas of challenging B_0 conditions (T_2*, DYNAMITE) compared to SH shimming (T_2*, SH).

NIH-PA Author Manuscript

NIH-PA Author Manuscript

NIH-PA Author Manuscript

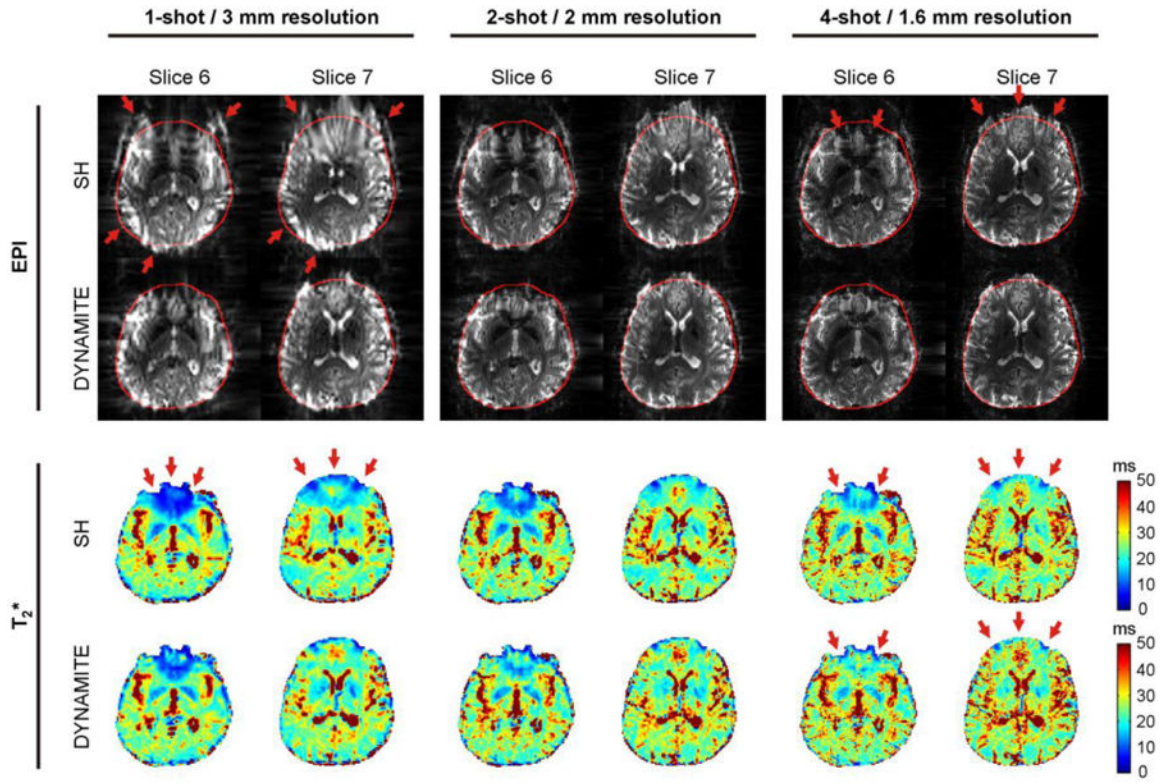

Fig. 5.

EPI and T_2* mapping quality as a function of image resolution and B_0 homogeneity. As expected, artifacts of EPI and T_2* mapping are reduced with increased spatial resolution (left-to-right: 1-shot to 4-shot at 3 mm to 1.6 mm, respectively). However, neither spatial deformations in EPI nor the macroscopic T_2* shortening are completely avoided with SH shimming even at the highest resolution applied in this study (EPI SH, right column). Only the combination of high resolution and DYNAMITE shimming was able to mitigate the artifacts in both EPI and T_2* maps (4-shot: EPI/T_2* DYNAMITE).

NIH-PA Author Manuscript

NIH-PA Author Manuscript

NIH-PA Author Manuscript

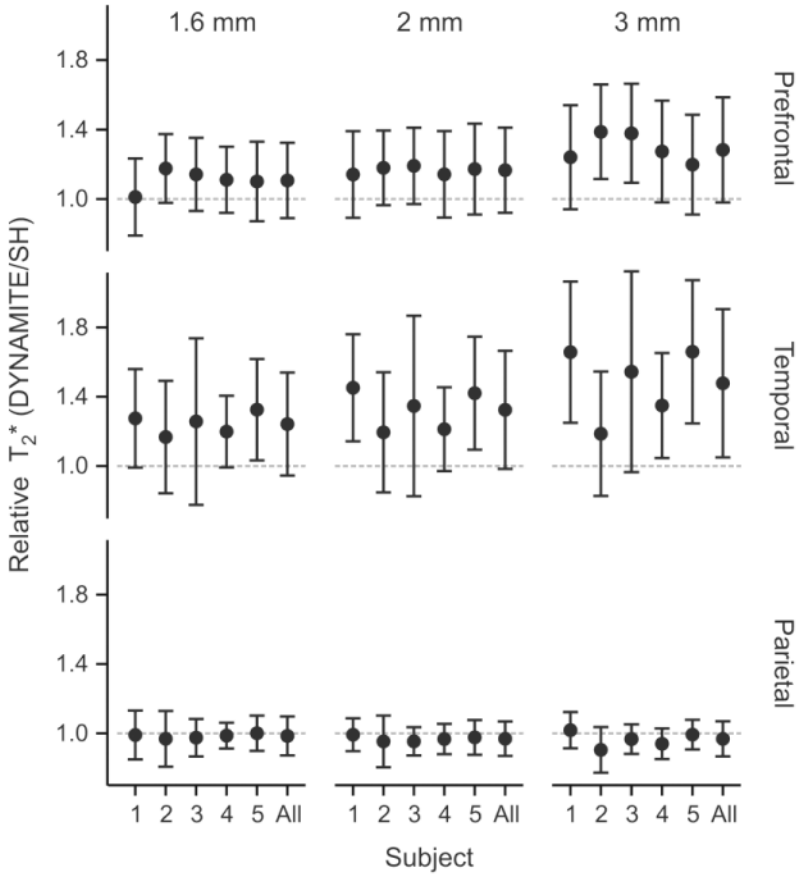

Fig. 6.

Estimated relative T_2* values (DYNAMITE/SH) in prefrontal cortex, temporal lobes and parietal lobe as a function of acquisition resolution, expressed as median ratio ± median absolute deviation. Similar T_2* values are obtained in the parietal lobe in which both shimming methods provide adequate B_0 homogeneity. Large T_2* improvements are achieved with DYNAMITE shimming in the prefrontal cortex and the temporal lobes, especially at coarser resolution, due an improved compensation of the complex B_0 terms encountered in these brain areas.

NIH-PA Author Manuscript

NIH-PA Author Manuscript

NIH-PA Author Manuscript

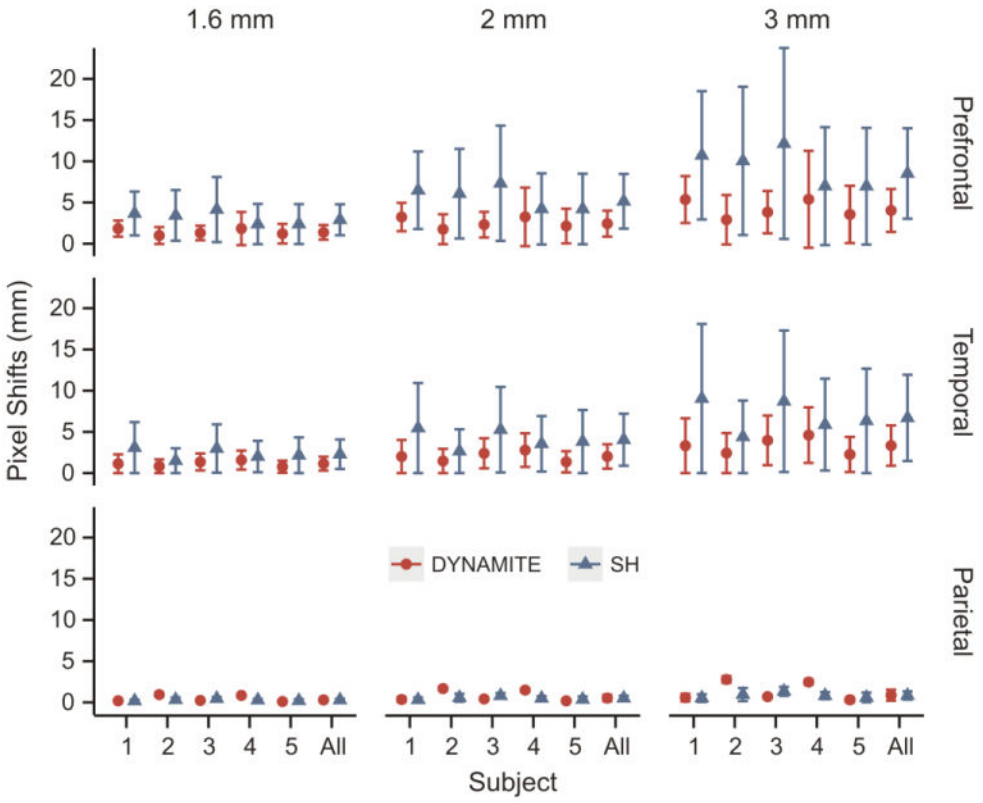

Fig. 7.

Estimated pixel shifts in EPI images as a function of spatial resolution and shim condition in the prefrontal cortex, temporal lobes and parietal lobe expressed as median pixel shift ± median absolute deviation. Large pixel shifts are observed with SH shimming in both the prefrontal cortex and the temporal lobes. Improvements are achieved with DYNAMITE shimming and finer image resolution. The combination of DYNAMITE shimming and high image resolution allows negligible pixels throughout the brain including difficult-to-shim areas such as the prefrontal cortex and the temporal lobes.

NIH-PA Author Manuscript
NIH-PA Author Manuscript
NIH-PA Author Manuscript

Table 1

Theoretical magnetic field homogenization of the human brain at 7 Tesla with different shimming techniques. Various order SH shimming was applied statically and dynamically assuming unlimited amplitude range. DYNAMITE shimming was based on experimentally calibrated basis fields with the applied MC setup including a ±1 A current limitation on all MC channels. Reported is the average standard deviation of the magnetic field distributions from 5 brains after shimming along with the width of the frequency distribution to include 80%, 85%, 90% and 95% of the brain voxels (all values in Hertz, mean ± SD).

Shim Method	SD	80%	85%	90%	95%
Static SH, 1st order	62,9 ± 5.3	143.6 ± 19.9	166.4 ± 17.5	208.5 ± 18.6	278.7 ± 24.3
Static SH, 2nd order	40.6 ± 3.6	77.8 ± 6.5	96.2 ± 7.5	121.9 ± 11.6	173.2 ± 17.4
Static SH, 3rd order	36.0 ± 3.8	63.0 ± 8.5	79.4 ± 9.2	106.3 ± 13.4	159.6 ± 22.9
Static SH, 4th order	30.8 ± 4.0	50.5 ± 8.3	63.4 ± 10.0	84.6 ± 12.0	131.9 ± 21.2
Static SH, 5th order	26,1 ± 3.9	38.9 ± 7.1	50.4 ± 9.1	67.4 ± 10.5	107.1 ± 17.0
Dynamic SH, 1st order	38.7 ± 1.4	83.0 ± 7.0	99.0 ± 10.1	118.3 ± 10.6	151.2 ± 10.1
Dynamic SH, 2nd order	28.8 ± 1.3	50.9 ± 3.3	62.6 ± 4.1	81.8 ± 5.2	122.3 ± 6.6
Dynamic SH, 3rd order	24.5 ± 1.8	47.3 ± 5.9	57.3 ± 6.8	71.4 ± 5.8	100.6 ± 8.2
Dynamic SH, 4th order	17.2 ± 0.9	29.3 ± 3.0	36.1 ± 3.5	47.3 ± 3.9	69.4 ± 4.1
DYNAMITE shim	13.5 ± 0.5	20.5 ± 1.7	26.1 ± 2.4	34.9 ± 3.0	52.9 ± 4.6

Neuroimage. Author manuscript; available in PMC 2016 January 15.

NIH-PA Author Manuscript
NIH-PA Author Manuscript
NIH-PA Author Manuscript

Table 2

Experimental magnetic field shimming for EPI and T_2* mapping of the human brain at 7 Tesla. Static SH and DYNAMITE shimming were applied to the slice slabs considered by EPI and T_2* mapping (compare Figs. 3/4). Notably all SH shim requirements stayed within the available dynamic range whereas the ±1 A current limitations for DYNAMITE shimming were regularly reached. Reported is the average standard deviation of the magnetic field distributions from 5 brains after shimming along with the width of the frequency distribution to include 80%, 85%, 90% and 95% of the brain slabs considered for EPI and T_2* mapping (all values in Hertz, mean ± SD).

Shim Method	SD	80%	85%	90%	95%
Static SH, 3rd order	32.3 ± 5.5	56.1 ± 7.9	71.8 ± 11.5	93.8 ± 14.0	138.7 ± 24.4
DYNAMITE shim	13.3 ± 1.7	24.9 ± 2.3	30.5 ± 33	38.5 ± 4.6	54.5 ± 8.2

Neuroimage. Author manuscript; available in PMC 2016 January 15.